THE EUROPEAN
PHYSICAL JOURNAL A

Constraining the nuclear spin distribution using improved ^{197}Au neutron resonance parameters

P. E. Koehler[a] , **J. L. Ullmann, A. J. Couture, S. M. Mosby**

Los Alamos National Laboratory, Los Alamos, USA

Communicated by Nicolas Alamanos

Abstract New neutron transmission data at resonance energies using a ^{197}Au sample were measured using an early version of the Device for Indirect Capture Experiments on Radionuclides (DICER), which is under development at the Los Alamos Neutron Science Center (LANSCE). These data were combined with previous neutron transmission and capture data in a simultaneous R-matrix analysis to extract improved neutron resonance parameters for this nuclide. As a result, total radiation widths, Γ_γ, were obtained for 33 $J = 1$ and 44 $J = 2$ ^{197}Au+n resonances. Γ_γ distributions for these two spins states were compared to distributions calculated according to the nuclear statistical model using published nuclear level density (NLD) and photon strength functions (PSF) measured using the Oslo technique. The calculated distributions were found to be narrower and the average values for the two spins states closer together than the data. The calculation can be brought into agreement with the data by substantial modifications to the spin distribution in ^{198}Au as a function of excitation energy. As far as we know, the spin distribution currently is otherwise poorly constrained. The modified spin distribution changes the shapes of the NLD and PSF extracted using the Oslo technique and so could have broad implications.

1 Introduction

Average s-wave neutron resonance spacings D_0 and total radiation widths $\langle \Gamma_{\gamma,0} \rangle$ are routinely used to calibrate nuclear level densities (NLDs) and photon strength functions (PSFs) obtained with the Oslo technique [1]. However, there is more information beyond D_0 and $\langle \Gamma_{\gamma,0} \rangle$, so it is possible to use additional pieces of the neutron resonance data to test other calibrations as well as assumptions inherent in the extraction

of NLDs and PSFs from the Oslo data. For example [2], the distribution of total radiation widths can be calculated, in the framework of the nuclear statistical model (NSM), using the same NLD and PSF which were calibrated using D_0 and $\langle \Gamma_{\gamma,0} \rangle$ from the same neutron resonance data set. Recently published NLDs [3] and PSFs [4] for ^{198}Au, together with improved Γ_γ values from our simultaneous R-matrix analysis of new neutron total cross section data and previous neutron total [5] and capture [6] data make possible such a test for ^{198}Au as described herein.

## 2 New ^{197}Au+n neutron transmission measurements

We have been developing [7] the Device for Indirect Neutron Capture Experiments on Radionuclides (DICER) at the Los Alamos Neutron Science Center (LANSCE), to tightly constrain (n,γ) cross sections on short-lived radionuclides by measurement and analysis of resonance neutron total cross sections on very small samples of the same nuclides.

As DICER is developed, we have been making test measurements with smaller and smaller samples. One of the first tests used a ^{197}Au sample which was 0.00169 at/b thick. A collimator 6 mm in diameter defined the neutron beam at the sample 30 m from the neutron-production target. Neutrons were detected with a ^{6}Li-glass scintillator 64.4 m from the neutron-production target. Separate measurements with no sample as well as with thick Bi, Cu, and Tm samples were made with the same apparatus to measure and subtract backgrounds and subsequently calculate the transmission (total cross section).

Data were taken at the standard- ($\Delta t_{PSR} = 125$ ns) and reduced-width ($\Delta t_{PSR} = 30$ ns) proton pulses from the proton storage ring (PSR) at LANSCE to quantify the improvement in resolution resulting from shorter pulses. Data taken

Fig. 1 ^{197}Au neutron capture data from n_TOF [6] (upper panel with scale on the right) and new transmission data from DICER (lower panel with scale on the left) in the energy range from 2.70 to 2.91 keV. Also shown are SAMMY R-matrix descriptions of the data using the latest ENDF parameters [9] (dashed red curves) and from this work (solid black curves). There are no GELINA transmission data in this energy range
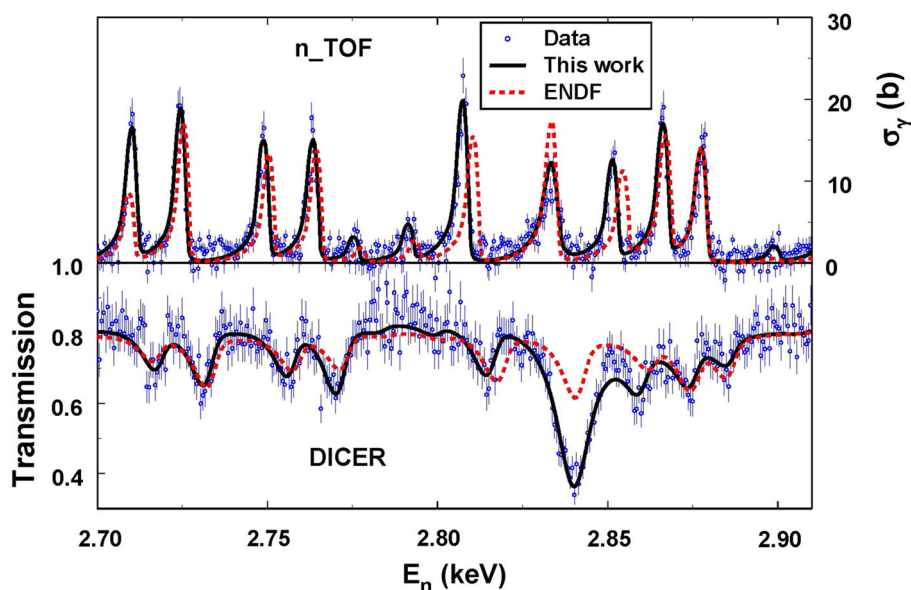
with the shorter pulse width had significantly improved resolution and so these data were used in the subsequent R-matrix analysis. The new neutron production target [8] currently being installed at LANSCE is expected to result in dramatically better resolution, especially at shorter PSR pulse widths, due to an improved, more compact, moderator.

Initial comparison of the new DICER data to the latest ENDF evaluation [9] revealed several differences. Therefore, a new R-matrix analysis was undertaken as described in the next section.

3 R-matrix analysis

A simultaneous R-matrix analysis of our new transmission data as well as recent transmission data [5] from GELINA and capture data [6] from n_TOF was undertaken using the R-matrix program SAMMY [10]. In total, 281 resonances were fitted between 4.9 eV and 5 keV. Good fits were obtained to all three data sets. In contrast, the latest ENDF [9] parameters provide a poor description of the data in many instances. Agreement between ENDF and the data is particularly poor over energy regions where there are no data from Ref. [5], for example as shown in Fig. 1. In addition, agreement between ENDF and the capture data is rather poor in many cases, even in energy regions where there are data from Ref. [5], as shown in Fig. 2.

For this work, we are concerned with resonances having firm spin assignments. Even in these cases, ENDF [9] resonance parameters often do not result in good fits to the capture data. For example the resonance near 293 eV has been assigned firm $J = 2$ [11,12], but as shown in Fig. 3 the latest ENDF parameters [9] result in a poor fit to the capture data. The resonance parameters of Ref. [12] result

in an even worse fit to the capture data for this and many other resonances. It appears that the relatively poor agreement between the capture data and ENDF and Ref. [12] for this and several other resonances resulted from restricting the Γ_γ values to a fairly narrow range. This common practice of restricting the range of Γ_γ values is motivated by theory (e.g. see Ref. [13]) and may be justified when the data are limited or of relatively poor quality. However, in the present case this practice not only results in poorer agreement with the neutron cross-section data but also nullifies the usefulness of the resulting resonance parameters for testing and improving theory.

Reliable Γ_γ values for testing the NLD and PSF data could be obtained only for the subset of resonances for which the spins were known and for which the neutron widths were large enough for Γ_γ to be determined with sufficient accuracy. Spins have been determined for 99 resonances below 2150 eV in Refs. [11,12] as given in Tables 1 and 2 of Ref. [12]. The 53 resonance spins in the former table were assigned in Ref. [12] whereas the 46 spin assignments in the latter table are from Ref. [11]. Of these 99 cases, there were 77 (33 $J^\pi = 1^+$ and 44 $J^\pi = 2^+$) resonances for which Γ_γ could be obtained with reasonable accuracy (relative uncertainty less than 25%) in this work.

Cumulative Γ_γ distributions for these two subsets of resonances are shown in Fig. 4. Quantitative comparison of these data to NSM predictions is facilitated by using the maximum-likelihood (ML) technique to calculate most likely values for the averages and widths of the Γ_γ distributions for each of the two spins. These distributions are expected [13] to be very close to Gaussian in shape (well described by χ^2 distributions with many degrees of freedom). Using Gaussian rather than a χ^2 distribution allows straightforward inclusion of uncertainties in the ML analysis [14]. Resulting values from

Fig. 2 ^{197}Au neutron capture data from n_TOF [6] (upper panel with scale on the right), new transmission data from DICER (middle panel with scale on the left), and transmission data from GELINA [5] (lower panel with scale on the right) in the energy range from 2.10 to 2.17 keV. Also shown are SAMMY R-matrix descriptions of the data using the latest ENDF parameters (dashed red curves) and from this work (solid black curves)
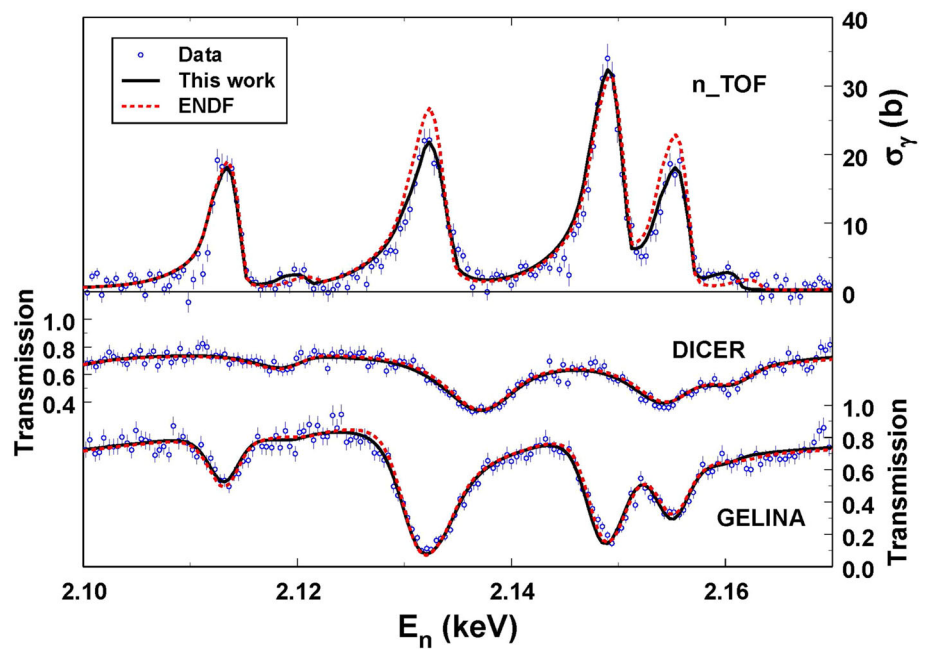

Fig. 3 ^{197}Au neutron capture data from n_TOF [6] (upper panel with scale on the right), new transmission data from DICER (middle panel with scale on the left), and transmission data from GELINA [5] (lower panel with scale on the right) in the energy range near the 293-eV $J = 2$ resonance. Also shown are SAMMY R-matrix descriptions of the data using the latest ENDF parameters [9] (dashed red curves) and from this work (solid black curves)
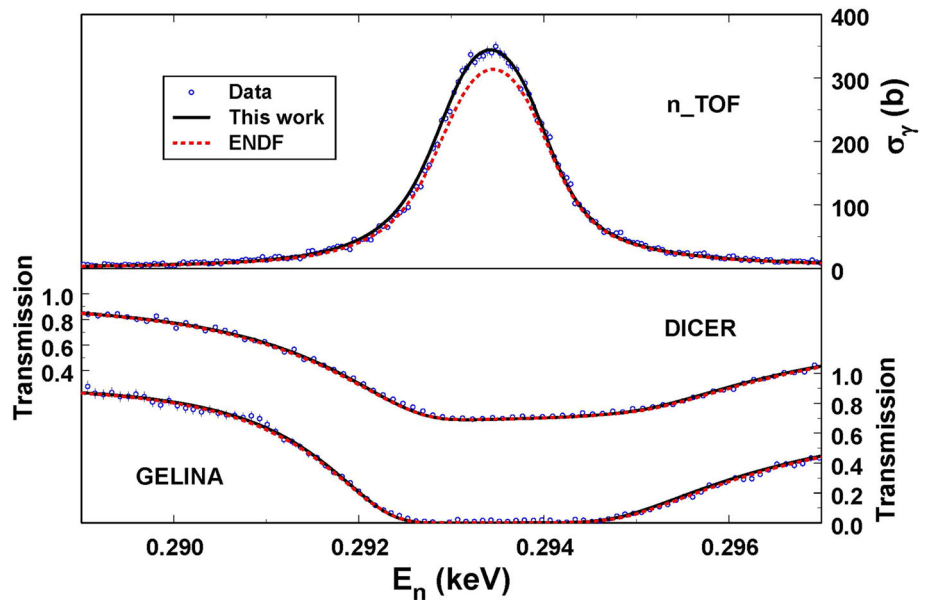
this ML analysis are given in Table 1. The second column in this table contains the difference between the mean values of the distributions for the two spins whereas columns 3 and 4 contain the standard deviations of the distributions for $J = 1$ and $J = 2$ resonances, respectively. The procedure for calculating Γ_γ distributions in the framework of the NSM and comparison of the results of these calculations to the data are described in the next section. We compare the NSM results to the measured difference between the means of the two distributions because each NSM calculation is normalized to the overall mean Γ_γ.

4 Statistical model calculation and results

Given a PSF and NLD, it is straightforward [2] to calculate Γ_γ distributions in the framework of the NSM. The total radiation width Γ_γ is the sum of all partial radiation widths $\Gamma_{\gamma\lambda f}(XL)$ between resonance λ and final level f which can be reached by a transition of type X (electric or magnetic) and multipolarity L,

$$\Gamma_\gamma = \sum_f \sum_{XL} \Gamma_{\gamma\lambda f}(XL).$$

Fig. 4 Measured (blue circles and red X's) and simulated cumulative total radiation-width distri-butions for ^{197}Au J=1 and 2 neutron resonances. The calculations were performed using the published Oslo NLD and PSF (short-dashed light blue and long-dashed light red curves) and modified NLD and PSF calibrated using alternative spin distribution A4 shown in Fig. 5 (dot-dashed dark blue and solid dark red curves)
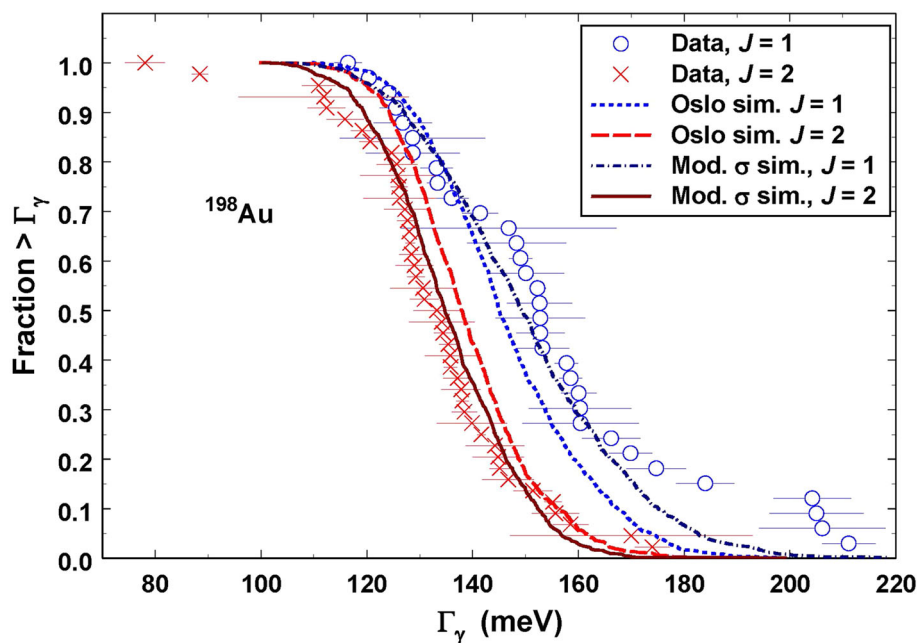

Table 1 Gaussian Γ_γ distribution parameters from ML analysis of the data, with one-standard-deviation uncertainties, (row 1) and NSM calculations (rows 2–6). σ_G is the standard deviation of the assumed Gaussian distribution

Case	$\langle \Gamma_{\gamma,0} \rangle_{J=1} - \langle \Gamma_{\gamma,0} \rangle_{J=2}$ (meV)	$\sigma_{G,J=1}$ (meV)	$\sigma_{G,J=2}$ (meV)
Data	21.8± 4.9	24.1± 3.1	16.3± 1.8
Oslo	7.7	14.8	12.5
A1	11.4	13.3	10.4
A2	13.4	22.2	14.7
A3	14.8	18.8	12.8
A4	13.5	23.7	16.6

The NSM assumes the partial radiation widths follow a Porter-Thomas distribution (PTD) [13] around their expectation value,

$$\langle \Gamma_{\gamma\lambda f} \rangle = \frac{f_{XL}(E_\gamma) E_\gamma^3}{\rho(E_\lambda, J_\lambda, \pi_\lambda)},$$

where $E_\gamma = B_n - E_f$ is the γ-ray energy, $\rho(E_\lambda, J_\lambda, \pi_\lambda)$ is the NLD of resonances with spin J_λ and parity π_λ at energy E_λ, and $f_{XL}(E_\gamma)$ is the PSF for XL transitions.

Calculating a Γ_γ distribution then involves the following steps. A complete level scheme above a critical excitation energy E_c is generated according to the NLD. Below E_c (0.626 MeV for ^{198}Au), values of E_f, J_f, and π_f determined from experiments are used. Spin and parity selection rules are properly taken into account for individual transitions. Partial radiation widths are then calculated by random sampling from PTDs characterized by the corresponding expectation values. To obtain a distribution of Γ_γ values, this process is repeated numerous times using the same level scheme but new PTD sampling each time.

Results of calculating Γ_γ distributions for 1^+ and 2^+ resonances in ^{198}Au using published NLDs [3] and PSFs [4] measured with the Oslo technique are compared to our new

data in Fig. 4. From this figure and the quantitative results in Table 1, it can be seen that the calculated distributions are significantly narrower and closer together than the data.

The NLD and PSF extracted from the Oslo technique was calibrated using (1) the known levels near the ground state, (2) the average resonance spacing for s-wave-resonances near the neutron separation energy, D_0, (3) the average total radiation width for these same resonances, $\langle \Gamma_{\gamma 0} \rangle$, and (4) a model for the spin distribution as a function of excitation energy. These calibrations affect the slopes of the NLD and PSF and consequently the widths of the Γ_γ distributions as well as the distance between the mean values of the distributions for the two spins. In the present case, the first three calibrations are fixed by data from previous (1) and the present (2 and 3) work. Below, we describe how the Oslo NLD and PSF can be adjusted, within the confines of the technique, the data, and the spin-distribution model, to obtain agreement between the NSM calculation and Γ_γ distribution data.

The fact that Γ_γ distributions have finite width is a consequence of Porter-Thomas fluctuations but the magnitude of the width (as well as the distance between the distributions for the two spins) depends on details of the NLD and PSF. Transitions to levels near the ground state tend to have the

Fig. 5 Various values of the spin-cutoff parameter, as a function of excitation energy, used in the NSM calculations of the Γ_γ distributions. See text for details
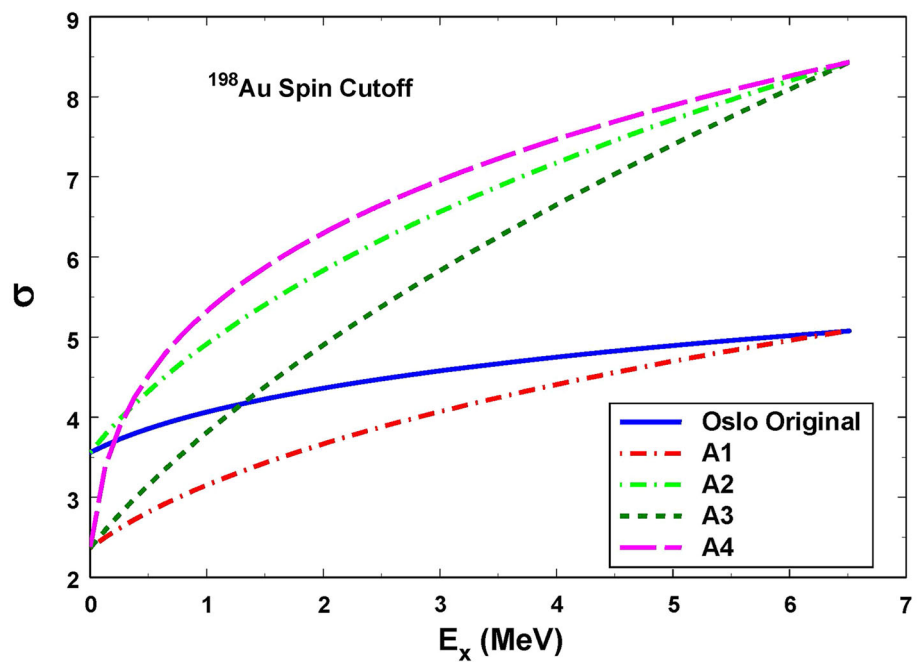
greatest influence on the width of the distribution because they have the largest partial widths. The spin distribution of the NLD can affect the width of the Γ_γ distributions in several ways. For example, increasing the number of levels of a given spin (to which resonance transitions can occur) near the ground state can make the distribution narrower because the fluctuations will be damped by averaging over more contributions. The spin distribution also affects the slope of the PSF, which affects the widths of the Γ_γ distributions. For example, a PSF with steeper energy dependence (due to a broader spin distribution at higher excitations) can lead to a wider Γ_γ distribution, by increasing the relative sizes of the largest partial widths.

The spin distribution of the NLD also affects the separation between the Γ_γ distributions for the two s-wave-resonance spins in at least two ways. First, the expectation value is inversely proportional to the average level density, $\rho(E_\lambda, J_\lambda, \pi_\lambda)$, for resonances of a given spin. Because there are more $J = 2$ than $J = 1$ resonances, the expectation value is smaller for the larger spin and hence the cumulative distribution for $J = 2$ is, on average, to the left of the $J = 1$ distribution in Fig. 4. In the present work, this component is fixed because the relative number of resonances of the two spins is obtained from our R-matrix analysis.

The second way the spin distribution affects the separation between the Γ_γ distributions for the two spins is through the relative number of $J = 0$ to $J = 3$ final states. This is because, assuming dipole transition dominate, only $J = 1$ ($J = 2$) resonances can decay to $J = 0$ ($J = 3$) levels. Therefore, increasing the number of $J = 0$ relative to $J = 3$ levels, especially near the ground state where the corresponding partial widths are larger, will increase the sepa-

ration between the two Γ_γ distributions. On the other hand, too many low-spin levels near the ground state can lead to a narrowing of the distributions as explained above. So, the spin distribution is constrained in opposite directions by the widths and relative spacing between the Γ_γ distributions for the two s-wave-resonance spins.

The spin distribution typically is parameterized in terms of the spin-cutoff parameter σ,

$$\rho_J = \frac{2J + 1}{2\sigma^2} e^{-\frac{J(J+1)}{2\sigma^2}} \rho,$$

where σ is a function of excitation energy. Within the framework of this model, we explored three changes to to spin distribution as a function of excitation energy to obtain better agreement with the Γ_γ distribution data shown in Fig. 4. Four models (A1 through A4) for the spin cutoff parameter as a function of excitation energy exploring these changes, as well as the model used in the Oslo analysis, are shown in Fig. 5.

First, we tried reducing the spin cutoff parameter at low excitation $\sigma(0)$, from the Oslo value of 3.56 to 2.37 (models A1, A3, and A4). As shown in Fig. 6, the known levels below $E_{cut} = 0.626$ MeV favor this change. As explained above, this change increased the separation between the simulated Γ_γ distributions for the two spins by increasing the relative number of $J = 0$ to $J = 3$ levels at lower excitation energies. Second, we explored increasing the spin cutoff parameter at the neutron separation energy (models A2, A3, and A4), $\sigma(Sn)$, from 5.08 to 8.43. As explained above, this change broadens the Γ_γ distributions. Third, we tried using a steeper energy dependence [15] of the spin cutoff parameter (model A4) rather than the more standard [16] energy dependence used in the Oslo analysis (and models A1, A2, and A3). This

Fig. 6 Spin distribution for known levels in ^{198}Au below $E_{cut} = 0.626$ MeV (black circles) together with the spin distribution used in Ref. [4] (dashed blue curve) and our fit to these data using the standard formula (solid red curve)
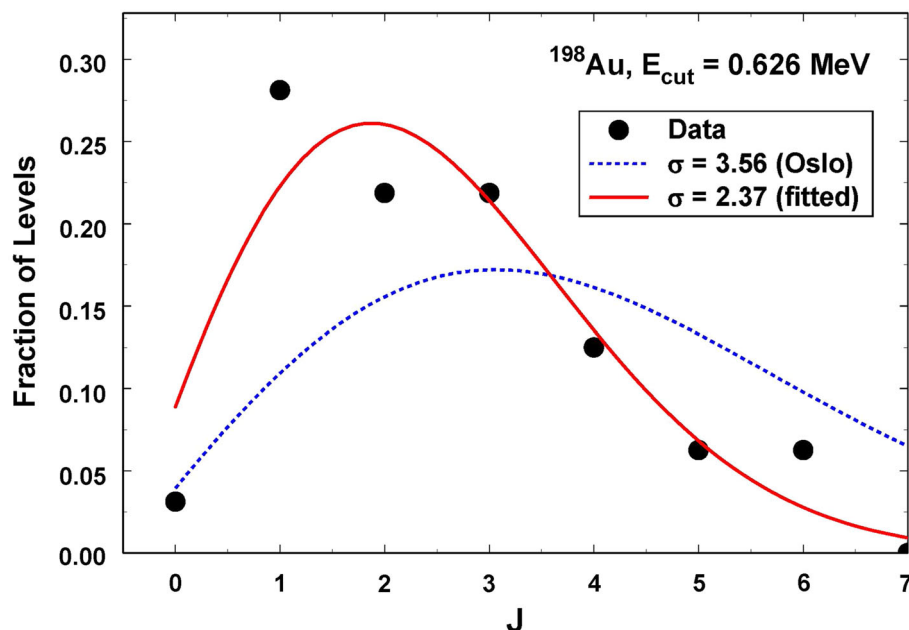
change also broadens the Γ_γ distributions. As far as we know, these changes are all within what is allowed by the available data.

As can be seen from Table 1, model A4 produces Γ_γ distributions in best agreement with the data, although models A2 and A3 also are withing two standard deviations of all three parameters extracted from the data. These results, together with the data shown in Fig. 6, suggest that $\sigma(0)$ ($\sigma(Sn)$) is significantly smaller (larger) than used in the Oslo analysis and hence both the NLD and PSF are steeper than the published versions [3,4].

It also is possible to broaden the NSM-calculated Γ_γ distributions by using a partial radiation width distribution broader than the PTD. Reduced neutron widths for nearby Pt isotopes have been shown [17] to have a broader distribution excluding the PTD with high confidence. However, changing the NSM calculation in this way does not affect the distance between the means of the distributions for the two spins and hence cannot by itself reconcile the NSM calculations with the data of the present work.

5 Conclusions

Distributions of total radiation widths for ^{197}Au neutron resonances were obtained from simultaneous R-matrix analysis of new data from DICER as well as previous data from n_TOF and GELINA. These data were compared to calculated distributions in the framework of the NSM using published NLDs and PSFs measured using the Oslo technique. There were significant differences between the measured and calculated distributions. We obtained agreement with the data by adjusting the spin distribution of the NLD. As far as we

know, the spin distribution is otherwise poorly constrained, except at very low excitation in ^{198}Au. The technique we used is applicable to other nuclides for which there are high-quality neutron-resonance data and could be used to obtain much better constraints on the nuclear spin distribution as a function of excitation energy. As the spin distribution affects the shapes of the NLD and PSF extracted using the Oslo technique, this work could have broad implications.

Data Availability Statement This manuscript has associated data in a data repository. [Author's comment: The data will be available in EXFOR, https://www-nds.iaea.org/exfor/.]

References

1. A.C. Larsen, M. Guttormsen, M. Krtička, B. E., A. Burger, A. Gorgen, H.T. Nyhus, J. Rekstad, A. Schiller, S. Siem, H.K. Toft, G.M. Tveten, A. Voinov, K. Wilan, Phys. Rev. C **83**, 034315 (2011)

2. P.E. Koehler, A.C. Larsen, M. Guttormsen, S. Siem, K.H. Guber, Phys. Rev. C **88**, 041305 (2013)

3. F. Giacoppo, F.L. Bello Garrote, L.A. Bernstein, D.L. Bleuel, T.K. Eriksen, A. Firestone, R.B. Gorgen, M. Guttormsen, T.W. Hagen, B.B. Kheswa, M. Klintefjord, P.E. Koehler, A.C. Larsen, H.T. Nyhus, T. Renstrom, E. Sahin, S. Siem, T. Tornyi, Phys. Rev. C **90**, 054330 (2014)

4. F. Giacoppo, F.L. Bello Garrote, L.A. Bernstein, D.L. Bleuel, A. Firestone, R.B. Gorgen, M. Guttormsen, T.W. Hagen, M. Klintefjord, P.E. Koehler, A.C. Larsen, H.T. Nyhus, T. Renstrom, E. Sahin, S. Siem, T. Tornyi, Phys. Rev. C **91**, 054327 (2015)

5. I. Sirakov, B. Becker, R. Capote, E. Dupont, S. Kopecky, C. Massimi, P. Schillebeeckx, Eur. Phys. J. A **49**, 144 (2013)

6. C. Massimi et al. (nTOF collaboration), Phys. Rev. C **81**, 044616 (2010)

7. A. Stamatopoulos, P. Koehler, A. Couture, B. DiGiovine, G. Rusev, J. Ullmann, Nucl. Instrum. Methods Phys. Res. A **1025**, 166166 (2022)

8. L. Zavorka, M.J. Mocko, P.E. Koehler, Nucl. Instr. Methods Phys. Res. A **901**, 189 (2018)

9. D. Brown, M. Chadwick, R. Capote, A. Kahler, A. Trkov, M. Herman, A. Sonzogni, Y. Danon, A. Carlson, M. Dunn, D. Smith, G. Hale, G. Arbanas, R. Arcilla, C. Bates, B. Beck, B. Becker, F. Brown, R. Casperson, J. Conlin, D. Cullen, M. Descalle, Nucl. Data Sheets **148**, 1 (2018)

10. N.M. Larson, Updated users' guide for SAMMY: multilevel r-matrix fits to neutron data using Bayes' equations. Tech. Rep. ORNL/TM-9179/R8, Oak Ridge National Laboratory (2008)

11. J. Julien, S.D. Barros, G. Bianchi, C. Corge, V.D. Huynh, G.L. Poittevin, J. Morgenstern, F. Netter, C. Samour, R. Vastel, Nucl. Phys. **76**, 391 (1966)

12. R.N. Alves, S.D. Barros, P.L. Chevillon, J. Julien, J. Morgenstern, C. Samour, Nucl. Phys. A **134**, 118 (1969)

13. C.E. Porter, R.G. Thomas, Phys. Rev. **104**, 483 (1956)

14. M. Asghar, C.M. Chaffey, M.C. Moxon, N.J. Pattenden, E.R. Rae, C.A. Uttley, Nucl. Phys. **76**, 196 (1966)

15. S.M. Grimes, J.D. Anderson, J.W. McClure, B.A. Pohl, C. Wong, Phys. Rev. C **10**, 2373 (1974)

16. T. von Egidy, D. Bucurescu, Phys. Rev. C **80**, 054310 (2009)

17. P.E. Koehler, F. Bečvář, M. Krtička, J.A. Harvey, K.H. Guber, Phys. Rev. Lett. **105**, 072502 (2010)